catalysts

MDPI

Article

Synthesis of High Crystalline TiO$_2$ Nanoparticles on a Polymer Membrane to Degrade Pollutants from Water

Kristina Fischer, Paulina Schulz, Igor Atanasov, Amira Abdul Latif, Isabell Thomas, Mathias Kühnert, Andrea Prager, Jan Griebel and Agnes Schulze *

Leibniz Institute of Surface Engineering (IOM), Permoserstr. 15, D-04318 Leipzig, Germany;
kristina.fischer@iom-leipzig.de (K.F.); paulina.diana.schulz2@gmail.com (P.S.); igor.atanasov@freenet.de (I.A.);
amira.abdullatif@iom-leipzig.de (A.A.L.); isabell.thomas@iom-leipzig.de (I.T.);
mathias.kuehnert@iom-leipzig.de (M.K.); andrea.prager@iom-leipzig.de (A.P.); jan.griebel@iom-leipzig.de (J.G.)
* Correspondence: agnes.schulze@iom-leipzig.de; Tel.: +49-341-235-2400

check for updates

Abstract: Titanium dioxide (TiO$_2$) is described as an established material to remove pollutants from water. However, TiO$_2$ is still not applied on a large scale due to issues concerning, for example, the form of use or low photocatalytic activity. We present an easily upscalable method to synthesize high active TiO$_2$ nanoparticles on a polyethersulfone microfiltration membrane to remove pollutants in a continuous way. For this purpose, titanium(IV) isopropoxide was mixed with water and hydrochloric acid and treated up to 210 °C. After cooling, the membrane was simply dip-coated into the TiO$_2$ nanoparticle dispersion. Standard characterization was undertaken (i.e., X-ray powder diffraction, scanning electron microscopy, X-ray photoelectron spectroscopy, water permeance, contact angle). Degradation of carbamazepine and methylene blue was executed. By increasing synthesis temperature crystallinity and photocatalytic activity elevates. Both ultrasound modification of nanoparticles and membrane pre-modification with carboxyl groups led to fine distribution of nanoparticles. The ultrasound-treated nanoparticles gave the highest photocatalytic activity in degrading carbamazepine and showed no decrease in degradation after nine times of repetition. The TiO$_2$ nanoparticles were strongly bound to the membrane. Photocatalytic TiO$_2$ nanoparticles with high activity were synthesized. The innovative method enables a fast and easy nanoparticle production, which could enable the use in large-scale water cleaning.

Keywords: photocatalysis; membrane; TiO$_2$ nanoparticles; carbamazepine; methylene blue

1. Introduction

The environment on earth is being more and more contaminated by anthropogenic pollutants [1,2]. Especially in water numerous contaminants like pharmaceuticals, endocrine disruptors, personal care products, and many more can be found and have an impact on animals and humans [3–5].

Due to the lack of elimination of these contaminants by conventional treatment technologies, other methods like advanced oxidation processes (AOPs) were considered [6]. Advanced oxidation processes (e.g., ozonation, Fenton, photo-Fenton, photocatalysis, radiation, sonolysis, and electrochemical oxidation) generate highly reactive oxygen species (ROS, like hydroxyl radicals, hydrogen peroxide, ozone, and superoxide anion radicals) with low selectivity. Complete mineralization of pollutants to carbon dioxide, water, and inorganic ions or acids is possible [6,7]. The photocatalyst titanium dioxide (TiO$_2$) has many advantages over other AOPs. Titanium dioxide is photo and chemical stable, of low cost, reusable, and non-toxic [8]. Further, no other toxic and expensive oxidants (like hydrogen peroxide or ozone) are needed. So far, TiO$_2$ has not yet been used in large-scale plants to remove pollutants

efficiently from water. The main challenge is to generate a low cost, long-term stable, and reusable system with a high activity to degrade organic contaminants.

The mode of application of TiO$_2$ is a crucial parameter as it already defines the degradation rate and success. Theoretically, the photocatalytic activity is the highest when using TiO$_2$ as nanoparticles in a suspension as the overall surface area can be immense. However, nanoparticles tend to agglomerate to larger particles (i.e., surface area is diminished) and after final cleaning the nanoparticles have to be removed extensively [9,10]. Binding TiO$_2$ to a support (e.g., membrane [11–14]) decreases the overall surface area but the degradation of pollutants can be executed in one step. Designing a porous support can overcome the surface area issues of a supported system. Membranes are ideal support systems as they are highly porous and can be produced easily, are cost effective, and exist in many different forms according to the need of the consumer. The pollutant is directly transported through the membrane to the photocatalyst for degradation. Slow transport of the pollutant to the photocatalyst (e.g., diffusion) is avoided. To generate a high surface area compound, the porosity should be high and the pore size low. Nonetheless, decreasing the pore size will increase the energy needed to operate the membrane system. Microfiltration membranes with a pore size of 0.22 and 0.45 µm have been successfully utilized [13,14].

Other parameters effecting the overall degradation rate are the geometric form (e.g., nanotubes, nanoparticles, nanorods, fibers, sheets, interconnected architectures) and size of TiO$_2$. The design also affects the surface area, thus the possible spots to generate radicals [15]. The goal is to generate a shape with a large surface area. One way is to decrease the size as the volume-to-surface area is increased. An additional positive effect when decreasing the size of nanoparticles is the shortening of the diffusion length for photogenerated electron-hole pairs (i.e., recombination is diminished) [16]. The morphology of TiO$_2$ also influences many other properties like electron transport velocity, charge separation, or charge recombination [17,18]. Using nanoparticles is an ideal combination of high surface area and low electron-hole pair recombination. We designed a simple synthesis method without using toxic chemicals at low temperatures to gain highly photocatalytic active TiO$_2$ nanoparticles [14].

The crystallite morphology was adjusted to form anatase, brookite, and rutile in a mixture, which increased the photocatalytic activity. By comparison of these three crystallite morphologies anatase possesses the highest photocatalytic activity [19]. As anatase is an indirect band gap semiconductor, the lifetime for photo excited electrons and holes is increased. Also, anatase exhibits a lower average effective mass of photo-generated electrons and holes. Thus, the electrons and holes will migrate faster from the bulk to the surface, which results in a low recombination rate [19]. The synthesis of pure brookite is technically difficult [20] so that only rare literature on the photocatalytic activity of brookite can be found [21–24]. In these studies brookite exhibits a higher photocatalytic activity because electrons are trapped, thus both electrons and holes are still accessible for reduction and oxidation reactions. A cathodic shift of the conduction band is also described so that interfacial electrons transfer to molecular oxygen [24]. The combination of these three crystallite morphologies has positive synergistic effects [25–30].

The crystallinity is another factor influencing the photocatalytic degradation rate of TiO$_2$ [31,32]. With high crystallinity the density of defects decreases. Defects act as recombination centers for electrons and holes, so they should be prohibited [16]. An increase in synthesis temperature results in an elevated crystallinity [30,33]. The upper synthesis temperature for generating TiO$_2$ nanoparticles directly on a polyethersulfone (PES) membrane has a limit at 130 °C as the polymer material will degrade above this temperature.

Therefore, the synthesis of TiO$_2$ nanoparticles is performed in the absence of the polymer membrane, and temperatures up to 210 °C were employed during synthesis. Highly crystalline TiO$_2$ nanoparticles with a high content of anatase (80%), a lower content of brookite (15%), and a very small content of rutile (5%) were synthesized. To still gain strongly attached, non-agglomerated TiO$_2$ nanoparticles on the membrane surface the nanoparticles were treated with ultrasound. Ultrasound generates a stable dispersion with smaller particles [34]. An additional dispergent is not needed. Thus,

upgrading to roll-to-roll modification is possible. Further, the membrane surface was modified with carboxylic groups to covalently attach and build up bonds between the surface carboxyl groups and TiO_2 nanoparticles. Commonly, polyacrylic acid (PAA) is attached to the membrane via different chemical grafting methods which use toxic chemicals [35]. Contrary, the carboxyl groups were introduced via electron beam modification with PAA using a green method. The resulting TiO_2-membrane system was characterized regarding scanning electron microscopy (SEM), X-ray powder diffraction (XRD), X-ray photoelectron spectroscopy (XPS), contact angle measurement, water permeance, and stability of the nanoparticle attachment to the polymer surface. The photocatalytic activity was investigated by degradation of methylene blue as well as carbamazepine in a batch reactor.

2. Results and Discussion

2.1. Crystal Phase, Crystallinity, and Crystal Size

The crystal phase, crystallinity, and crystal size depend on the used synthesis parameters such as acid concentration, temperature, and synthesis time [14,36–38]. In a previous study [14] it was observed that TiO_2 with the main portion being anatase, a low portion of brookite, and a scarce content of rutile gained the highest photocatalytic activity. This composition was achieved by using a low hydrochloric acid concentration of 0.25 M during synthesis [14]. Here, we decreased the acid concentration to 0.1 M as the activity further increased (T = 120 °C, degradation of methylene blue: first-order rate constant $k_{0.1M}$ = 0.0504 min^{-1} and $k_{0.25M}$ = 0.0456 min^{-1}). The crystal phase composition changed only marginal. In addition, it was exhibited in the former study [14] and it is well-known in literature [38] that the crystallinity and crystal size increase with rising synthesis temperature. The crystal phase, crystallinity, and crystal size were observed with XRD (X-ray powder diffraction). The direct analysis of the crystal morphology on the PES membrane is not feasible as the content of TiO_2 is too low to gain sufficient signals. Therefore, the powder of TiO_2 nanoparticles was analyzed via XRD.

In contrast to our previous study, we now designed a synthesis procedure (see Section 3 for details) which allows also to use temperatures higher than 130 °C. The membrane was not present during high temperature treatment as it had been before [14]. In Figure 1a, the crystal pattern for TiO_2 nanoparticles synthesized at temperatures between 70 and 210 °C is shown. The peaks get more intense and sharper with increased temperature. Especially the signals of anatase (101)/brookite (120) show an elevation of intensity. Rutile (110) only appears at 210 °C with a sharp and intense peak. This was confirmed by synthesis repetition and evaluation of the crystal patterns via XRD. A further indication for an elevation in crystallinity is the trend of evolution of the crystal size. In Figure 1b, the crystal size against the temperature is shown. A clear trend of increasing crystal size with raised synthesis temperature was observed. This trend can be also found in literature [37,39] and in the former study [14]. The anatase crystal size elevates from 4 nm to 10 nm when the synthesis temperature is increased from 70 °C to 210 °C. The rutile crystal size (33 nm) is significantly larger than brookite and anatase crystals (was confirmed by synthesis repetition). The brookite crystal size increases over the whole temperature range from 5 nm to 9 nm with an intermediate decrease in between 90 °C and 150 °C. The intermediate decrease could arise from the calculation of the crystal size. The peaks were fitted (error of 5 to 8%) in order to gain the full width at half maximum.

The crystal composition does not change significantly with varying temperature (see Figure 1c). The anatase content shifts from 65 to 85%, while the brookite content varies between 15% and 37%. Rutile only appears at 210 °C with a content of only 5%. An intermediate decrease of the anatase content in between 90 °C and 150 °C arises, while brookite is increasing. Again the fitting of the peaks (error of 5 to 8%) could be an explanation for this anomaly.

The three modifications of TiO_2 are generated due to divers linking of TiO_6^{2-} octahedra [36,37,40–42] either by solid-state rearrangement for anatase or dissolution precipitation reaction for rutile [39]. Hereby, anatase exists of edge-sharing TiO_6^{2-} octahedra, while rutile shares an edge along the c-axis to form chains and corner-shared bonds among these chains, and brookite shares both edges and corners [37].

The mechanism of crystal formation due to combination of TiO_6^{2-} octahedra has been investigated elsewhere and uses different theories like the thermodynamic or the kinetic approach [36,43], while other theories discuss the amount of OH^- present at different conditions [41,42].
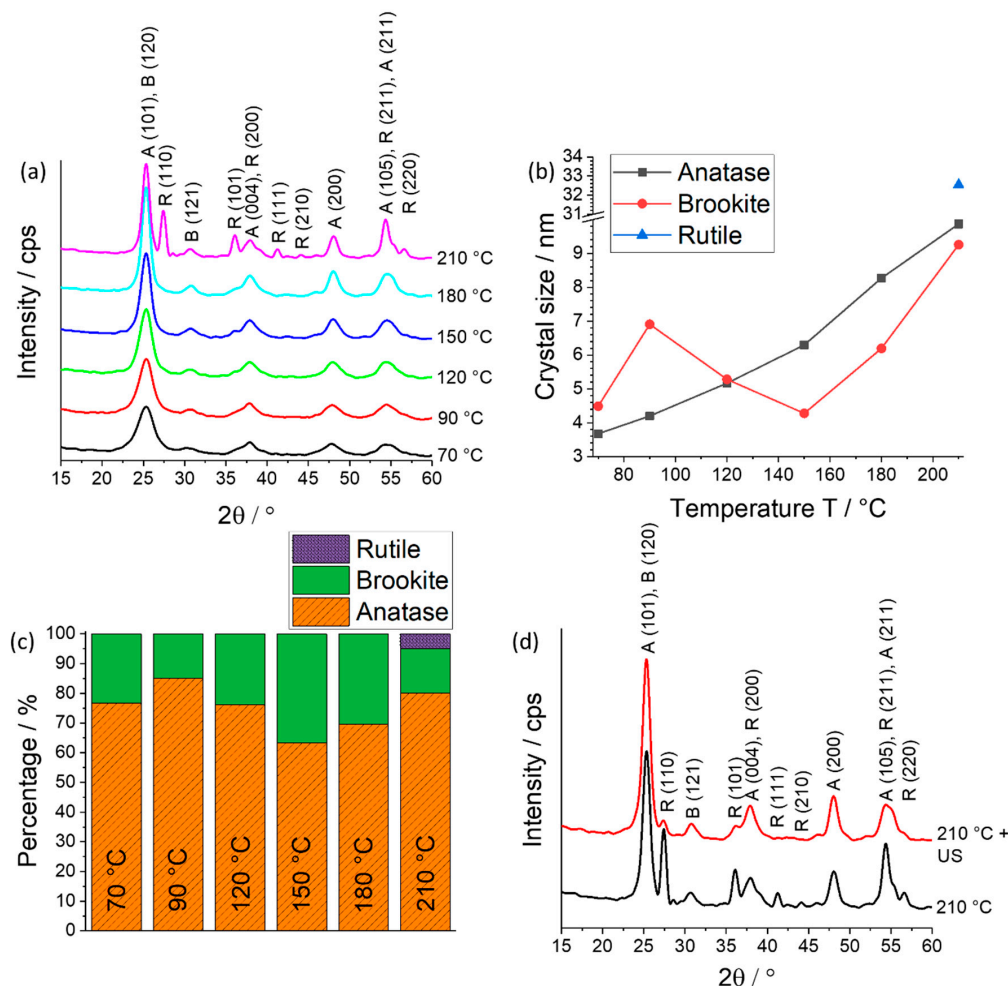

Figure 1. (**a**) XRD (X-ray diffraction) pattern of TiO_2 nanoparticles synthesized at different temperatures. (**b**) Crystal size against the synthesis temperature calculated by the Scherrer formula. (**c**) Percentage of phase type of TiO_2 nanoparticles prepared at different temperatures. (**d**) Comparison of the XRD pattern of TiO_2 nanoparticles synthesized at 210 °C with and without ultrasonic treatment. The XRD pattern were smoothened with a 17 point FFT (fast Fourier transform filter).

The acidity dictates the amount of formed OH^- ligands. At low acid concentration more OH^- ligands can be generated so that edge-sharing of TiO_6^{2-} octahedra is much more likely to occur during dehydration reactions and anatase is formed [37]. The generation of mainly anatase and almost no rutile can be also explained by the different mechanism of crystallization (solid-state mechanism for anatase and dissolution precipitation mechanism for rutile [39]). Titania only solubilizes at high acid concentrations as the surface becomes protonated and a dissolution precipitation process is possible to form rutile. The dissolution precipitation mechanism has no effect here as a very low concentration of acid was used.

Another factor to influence the generation of different crystal morphologies is the temperature. Again, the influence of OH^- can be taken into account as it changes according to the equilibrium law (Le Chatelier's principle). The concentration of OH^- decreases with lower temperatures [44] so that at low temperatures and high acid concentrations rutile was formed in the previous study [14]. Here,

with a very low concentration of acid the amount of OH^- is already too high to generate rutile next to anatase even at a higher temperature. The appearance of rutile at a high synthesis temperature can be associated to the growth of the crystals as there is a critical size for anatase and brookite to transform to rutile at a certain crystal size [14,36]. With increasing crystal size the crystals become unstable, migrate, and align, so that an in situ rearrangement of the lattice leads to a transformation to rutile.

For better distribution of the TiO_2 nanoparticles on the membrane (see Section 2.2) the dispersion containing TiO_2 nanoparticles was treated with ultrasound. Afterwards, the XRD pattern was investigated and is shown in Figure 1d. The intensity of the rutile peak declines, because the crystal size of rutile decreases from 32.5 nm to 19.3 nm, while the crystal size of anatase and brookite did not change significantly. Ultrasound generates acoustic cavitation which leads to the formation, growth, and implosive collapse of bubbles in a liquid. Due to implosive collapse adiabatic compression and shock waves form within the gas phase of the collapsing bubble. Large crystals (here rutile) can break up [45]. The content of rutile did not change due to the ultrasound treatment.

2.2. TiO$_2$ Nanoparticle Distribution on the Polymer Membrane

After preparation of the nanoparticles they were immobilized on a polymer membrane surface by dip-coating (see Section 3.2). The nanoparticle distribution and content depends on the temperature of synthesis, membrane pre-modification, and TiO_2 nanoparticle treatment.

When comparing the synthesis temperatures the coverage of the membrane surface with TiO_2 nanoparticles is the highest at a temperature of 120 °C (see Figure 2). This is consistent with the titanium content observed via XPS (X-ray photoelectron spectroscopy, Figure 3), where the membrane dip-coated with TiO_2 nanoparticles synthesized at 120 °C has the highest amount of titanium. Below 120 °C smaller particles were generated, while at temperatures above 120 °C the particles are larger but tend to agglomerate, and blank spots of the membrane can be observed.
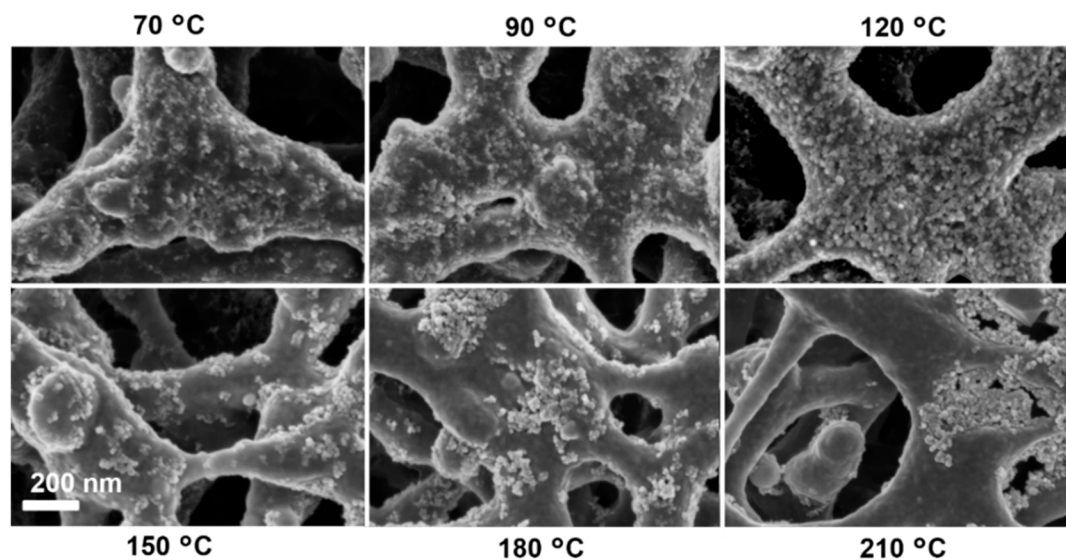

Figure 2. SEM (scanning electron microscopy) image of PES (polyethersulfone) membrane with TiO_2 nanoparticles synthesized at different temperatures (70 °C, 90 °C, 120 °C, 150 °C, 180 °C, and 210 °C).

In order to gain a completely covered membrane surface with TiO_2 nanoparticles two variations of the method were undertaken. Before dip-coating in the TiO_2 nanoparticle suspension the membrane was modified with PAA and electron beam in order to generate carboxyl groups (COOH) on the membrane surface (further on referenced to as 210 °C + COOH). For this, the membrane was dipped into a 0.01% PAA solution, transferred to a glass plate, and irradiated with an electron beam at 100 kGy.

After washing in water for 3 × 30 min the membrane was dried. The PAA with its carboxyl groups is covalently bound to the membrane via this method [46].
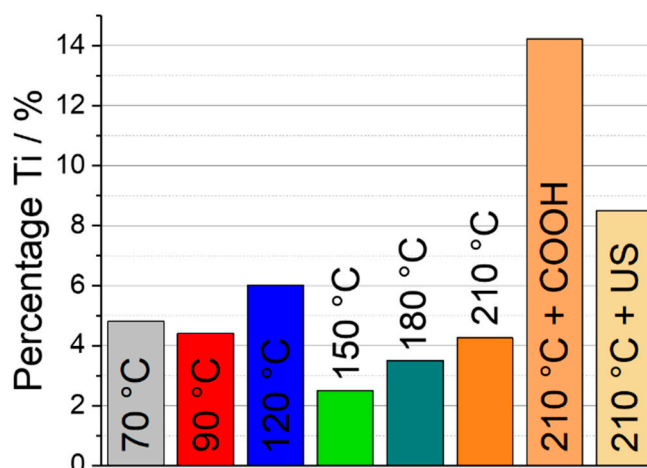

Figure 3. Titanium content in percentage on the PES membrane with TiO$_2$ nanoparticles synthesized at different temperatures (70 °C, 90 °C, 120 °C, 150 °C, 180 °C, and 210 °C) and modified with carboxyl groups prior to the dip-coating (210 °C + COOH) and modified with ultrasound (210 °C + US). The titanium content was determined by XPS.

The TiO$_2$ nanoparticles coordinate via Ti^{4+} and an electronegative group like oxygen atoms or the hydrogen bond between the surface hydroxyl group of TiO$_2$ and oxygen groups of the polymer [47]. TiO$_2$ can undergo different kind of bonding (e.g., monodentate, bridging bidentate, and chelating bidentate) [48] with the carboxyl groups on the membrane. In addition, the TiO$_2$ nanoparticle suspension was additionally treated with ultrasound (further on referenced to as 210 °C + US). As already described in Section 2.1, particles can break up due to ultrasound [45] and a homogeneous and stable suspension was generated. Both modifications succeeded to gain a complete coverage of the membrane with TiO$_2$ nanoparticles (Figure 4). Additionally, the amount of titanium observed via XPS increased significantly from 3% to values of 14% and 9% for the 210 °C + COOH and 210 °C + US method, respectively (Figure 3). Consequently, both variations were successful to gain a fine distribution of nanoparticles on the rough membrane surface. Furthermore, the polymer surface was completely covered by the nanoparticles and no voids or large agglomeration were detected.
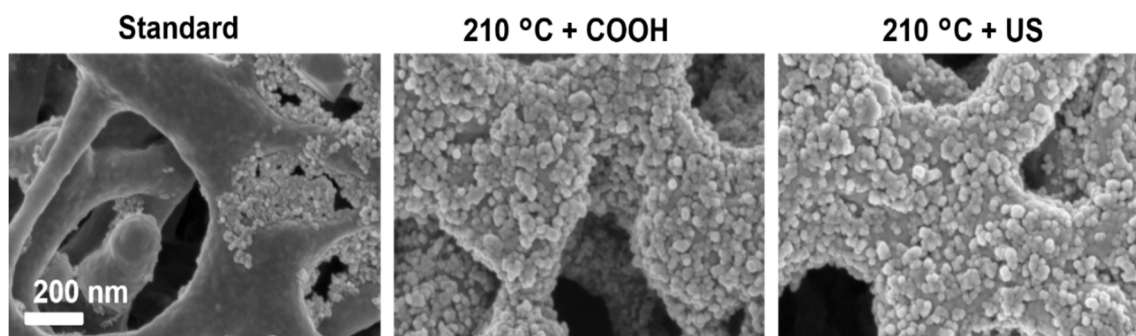

Figure 4. SEM image of a PES membrane with TiO$_2$ nanoparticles synthesized at 210 °C. Within the standard method no further modification of either membrane or nanoparticles was applied. The 210 °C + COOH method implemented COOH-groups via electron beam on the membrane before dip-coating. With the 210 °C + US method the nanoparticles in suspension were treated with ultrasound.

2.3. Water Permeance and Hydrophilicity

The performance of the membrane after modification was investigated by analyzing the water permeance and water contact angle (Figure 5).
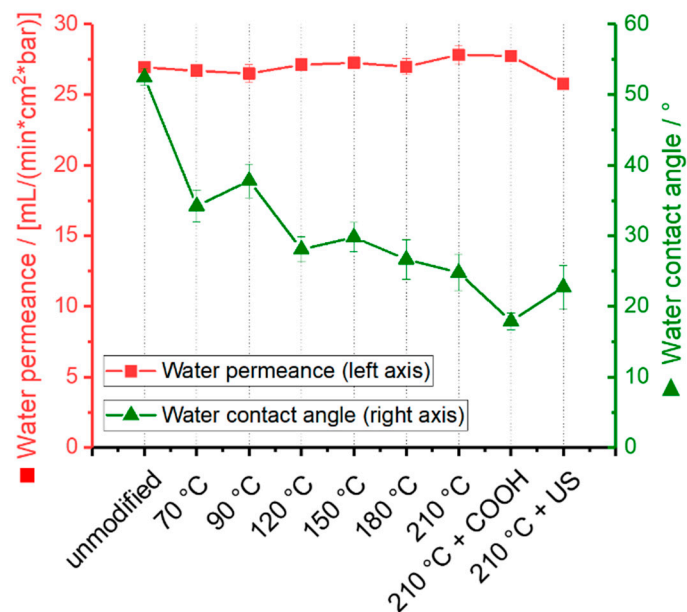

Figure 5. Water permeance (red, **left**) and water contact angle (green, **right**) of differently treated membranes (unmodified PES membrane, PES membrane with TiO_2 nanoparticles synthesized at different temperatures: 70 °C; 90 °C; 120 °C; 150 °C; 180 °C; 210 °C or modified with ultrasound: 210 °C + US, PES membrane modified with carboxyl groups prior to the dip-coating of TiO_2 nanoparticles: 210 °C + COOH.

The water permeance does not significantly change although a layer of TiO_2 nanoparticles has been attached to the pore surface of the membrane. The pore size is in the micrometer range, thus the influence of a thin nanometer thick layer of TiO_2 nanoparticles (d = 20–40 nm) is not significant as it has been also observed in previous studies [13,14]. Additionally, the effect of decreasing water contact angle (see below) plays a role and can improve the water permeance while the particle coverage slightly decreases the pore size and compensates the effect. The water contact angle decreases when TiO_2 nanoparticles were attached to the membrane from 52° to 34° for the unmodified and for the membrane with TiO_2 nanoparticle synthesized at 70 °C, respectively. A slight decrease regarding the contact angle at higher synthesis temperature is visible (from 34° at 70 °C to 24° at 210 °C). The membrane becomes more hydrophilic due to TiO_2 nanoparticle attachment, as it is well known from literature [13,14]. Values below 30° indicate a highly hydrophilic membrane. A hydrophilic membrane is preferable when working in water and is identified to prevent organic fouling [49,50]. The COOH-coated membrane with TiO_2 nanoparticles synthesized at 210 °C has the lowest contact angle with 18° as the TiO_2 nanoparticles are well distributed and COOH-modification itself hydrophilizes the membrane [51].

2.4. Stability of TiO_2 Nanoparticles on the Membrane

In order to not release nanoparticles into the environment, strong bonding of TiO_2 nanoparticles to the membrane is important. The membrane with TiO_2 nanoparticles underwent high shear stress while water was flowing by parallel to the surface at 30 bar in a cross-flow mode for one hour. After having passed the membrane, the titanium content of the water was analyzed by ICP-OES (inductively coupled plasma optical emission spectrometry). However, no titanium could be found in the water. Further, the surface of the membrane was analyzed via SEM and XPS before and after stability tests

(Figure 6). A possible loss of TiO$_2$ nanoparticles due to high cross-flow could not be observed for the 210 °C + COOH and 210 °C + US sample. The TiO$_2$ nanoparticles are strongly bound to the PES membrane surface either via Ti^{4+} and an electronegative group like oxygen molecules of PES or the carboxyl group or the hydrogen bond between the surface hydroxyl group of TiO$_2$ and oxygen groups of PES or the carboxyl group [47]. The membrane with TiO$_2$ nanoparticles immobilized via the standard method lost TiO$_2$. This can be only observed taking the XPS data. The SEM images show only a small portion of the sample. The loss is probably due to the agglomeration of TiO$_2$ nanoparticles, which wear off more easily. The above-described bonding forces cannot act. The 210 °C + COOH and 210 °C + US synthesis methods are therefore preferred as they give strongly bound TiO$_2$ nanoparticles on the surface.
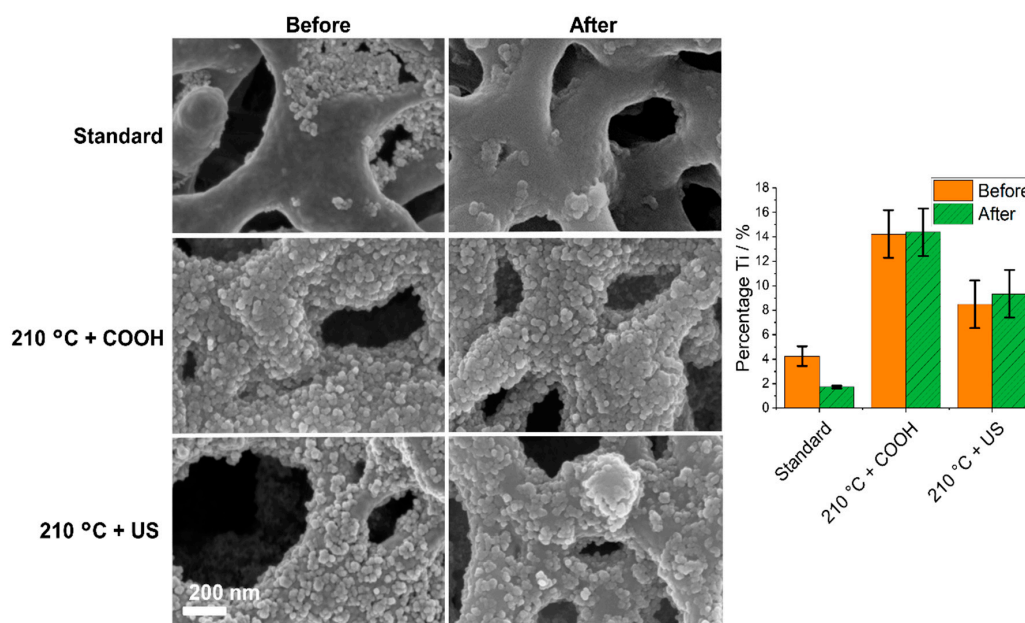
Figure 6. SEM images of the membrane surface (**left**) and percentage of titanium (**right**) on the membrane before and after stability test for the membrane modified with TiO$_2$ nanoparticles via the standard 210 °C, 210 °C + COOH, and 210 °C + US method.

2.5. Photocatalytic Activity

The photocatalytic activity was observed by degrading methylene blue (13 mg L^{-1}) in a simple batch reactor. The membrane with TiO$_2$ nanoparticles was placed in a six-well plate and filled with 4 mL of methylene blue solution. Before photocatalytic degradation dark adsorption was performed until no further methylene blue was adsorbed. Samples were taken periodically. Methylene blue is a model compound commonly used to characterize the photocatalytic performance [52–55]. A high concentration of methylene blue was chosen to generate slow degradation rates in order to be able to monitor the reaction with reduced error.

An elevated degradation velocity of methylene blue was observed (see Figure 7a,b) with increasing synthesis temperature of TiO$_2$ nanoparticles. At 70 °C a period of 100 min is required to degrade methylene blue completely, while at 210 °C after only a third of the time (30 min) methylene blue was totally removed. The reaction rate constant, which was calculated by plotting log(c/c$_0$) versus time and estimating the slope of the regression line, enhances exponentially (Figure 7b) with increasing synthesis temperature. A high rate constant demonstrates a fast degradation of a pollutant. At 70 °C the rate constant has a value of 0.02 min^{-1} and increases to 0.11 min^{-1} at 210 °C synthesis temperature. This is not consistent with the coverage of TiO$_2$ nanoparticles on the membrane at different temperatures (see Section 2.2). At 210 °C synthesis temperature, the membrane is only partially covered and

agglomerates of TiO_2 nanoparticles were formed. The membrane with TiO_2 nanoparticles generated at 120 °C shows better coverage with no empty spots and should therefore degrade methylene blue with the fastest rate. Taking the results from the XRD (Section 2.1), the crystallinity increases by elevating the temperature used for the formation of TiO_2 nanoparticles. An increase in crystallinity has many improving effects on the photocatalytic activity [14,31,32]. The density of defects does decrease due to a high crystallinity. The electrons and holes can recombine at defects and shall be diminished [16]. As the crystallinity increases with temperature elevation the number of defects reduces, electron-hole-pair recombination is decreased, thus more OH^- radicals can be formed and react to degrade methylene blue. Thus, the effect of crystallinity increase has a much higher impact on the photocatalytic degradation compared to the coverage of the membrane.

The dark adsorption of methylene blue was also analyzed and displayed in Figure 7b. Overall, the methylene blue adsorption increased with enhanced temperature of TiO_2 formation. The adsorption affinity effects the photocatalysis since with high adsorption the degradation rate is increased [56]. Methylene blue, as a cationic dye, likely adsorbs on a negatively charged surface like TiO_2 [57].
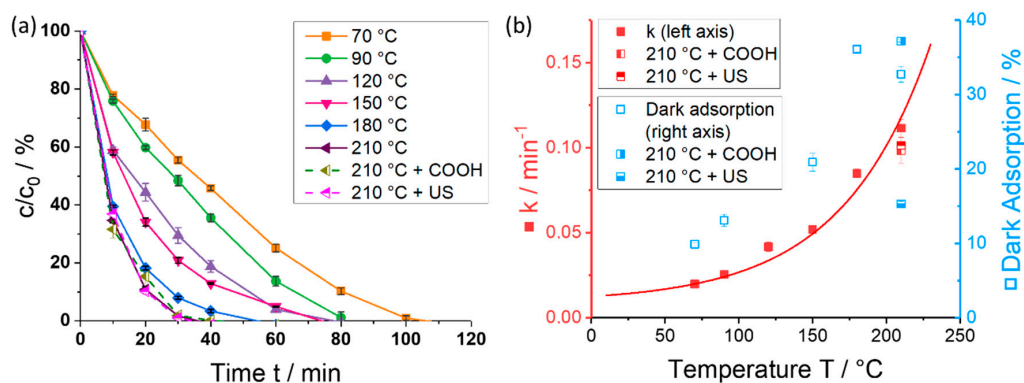

Figure 7. (**a**) Photocatalytic degradation of methylene blue (13 mg L^{-1}) over time and (**b**) reaction rate constant of the photocatalytic degradation and dark adsorption for differently synthesized membranes (unmodified PES membrane, PES membrane with TiO_2 nanoparticles synthesized at different temperatures: 70 °C; 90 °C; 120 °C; 150 °C; 180 °C; 210 °C or modified with ultrasound: 210 °C + US, PES membrane modified with carboxyl groups prior to the dip-coating of TiO_2 nanoparticles: 210 °C + COOH).

The TiO_2 nanoparticle distribution was increased (as mentioned and shown in previous sections) by pretreating the membrane with carboxyl groups or pretreating the TiO_2 nanoparticles with ultrasound before dip-coating to the membrane (210 °C+ COOH and 210 °C + US). An increased degradation rate was expected but not found (Figure 7a,b). The degradation rate does not change significantly, as the degradation velocity is too high to measure any differences. Therefore, another molecule (carbamazepine) and a higher concentration (25 mg L^{-1}) were chosen to slow down the degradation velocity, and to analyze a difference in photocatalytic degradation between the PES membrane with TiO_2 nanoparticles synthesized at 210 °C, the 210 °C + COOH and 210 °C + US sample. Carbamazepine is an antiepileptic drug, which is commonly found in surface and waste water [58,59]. Different molecules show divers degradation rates as the initial oxidation route, and eneration of photo-transformed intermediates are varied [60,61]. Carbamazepine degradation velocity was expected to be lower as photocatalytically generated by-products of carbamazepine (i.e., acridine) absorb light in the UVA region and compete with carbamazepine for oxidation [62].

Dark adsorption of methylene blue decreased distinctly for the 210 °C + US sample, while it increased slightly analyzing the 210 °C + COOH sample. Again, the charge of the membrane surface (after COOH modification) could be the reason for a higher adsorption compared to the membrane without COOH functional groups.

The three synthesis methods lead to clearly visible differences in degradation velocity when carbamazepine is degraded (Figure 8a). The ultrasonic treated TiO_2 nanoparticles on the membrane (210 °C + US) degrade carbamazepine with the highest speed, while the standard method (210 °C) led to the slowest rate. The dark adsorption for all three methods is similar (7.5% ± 0.7%—standard 210 °C, 10.3% ± 1.3%—210 °C + COOH method, and 3.9% ± 1.1%—210 °C + US method), where again the 210 °C + COOH method has the highest adsorption while the ultrasonic treated TiO_2 nanoparticle on the membrane (210 °C + US) has the lowest adsorption. The distribution of the TiO_2 nanoparticles on the membrane has an impact on the photocatalytic performance. Evenly distributed TiO_2 nanoparticles without agglomerates and blank spots on the membrane surface (210 °C + COOH, 210 °C + US) show an improved photocatalytic degradation.
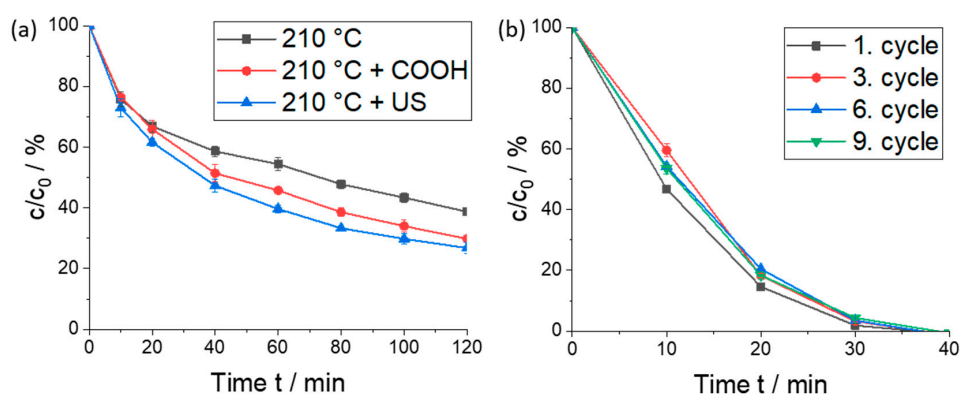

Figure 8. (**a**) Photocatalytic degradation of carbamazepine (25 mg L^{-1}) over time for PES membrane (unmodified and modified with carboxyl groups prior to the dip-coating—210 °C + COOH) with TiO_2 nanoparticles synthesized at 210 °C and modified with ultrasound (210 °C + US). (**b**) Photocatalytic degradation of methylene blue (13 mg L^{-1}) for up to nine cycles with the 210 °C + US membrane.

The long-term usability of the membrane in degrading pollutants from water has been tested by degrading methylene blue repeatedly for up to nine times (Figure 8b). The membrane with TiO_2 nanoparticles clearly does not show any loss in photocatalytic activity after nine cycles. This indicates a stable combination of the membrane with TiO_2 nanoparticles over long time usage. Ultraviolet light can damage the polymer membrane. But TiO_2 will act as a UV protective layer [63]. Further, it can be concluded that the polymer membrane was also not degraded by TiO_2. The TiO_2 nanoparticle will not degrade the polymer as long as there are molecules to attack in solution. Ultraviolet radiation was stopped after complete degradation of methylene blue.

3. Materials and Methods

3.1. Materials

A PES membrane (0.22 μm, Millipore Express® PLUS membrane GPWP) was used from Merck Millipore, Billerica, MA, USA. Hydrochloric acid (37%) and titanium(IV) isopropoxide (TTIP, 97%) were acquired from Sigma–Aldrich, Steinheim, Germany and methylene blue (96+%) from Acros Organics (Fisher Scientific, Waltham, MA, USA). Polyacrylic acid (M = 1800 g mol^{-1}) was supplied from Sigma–Aldrich, Steinheim, Germany. Milli-Q water was obtained from Milli-Q integral system (EMD Millipore, Billerica, MA, USA).

3.2. Nanoparticle Synthesis on the Membrane

A beaker was filled with Milli-Q water (80 mL in total), TTIP (4 mL), and 37% hydrochloric acid (0.1 M). The beaker was closed and stirred for 15 min at room temperature. Afterwards, the beaker was placed in the oven for 20 h at different temperatures (70–210 °C). The beaker was cooled for 2 h

and stirred or treated with an ultrasonic probe for 90 s and at 40 W (Sonoplus, HD2200 Generator, KE76 probe, BANDELIN electronic GmbH & Co., KG, Berlin, Germany), subsequently.

A membrane (9 × 9 cm) was placed (with the side with smaller pores facing downwards) into the solution and was shaken for 5 min. Afterwards, the membrane was washed with Milli-Q water for 3 × 30 min and dried.

The surface modification of a membrane with a polymer (here polyacrylic acid, PAA) and electron beam in order to gain a surface with carboxyl groups (COOH) is described elsewhere [46]. To make it short, the membrane was dipped into an aqueous solution of 0.01% PAA and irradiated by electron beam on a glass plate in wet state at 100 kGy. Afterwards, the membrane was washed with Milli-Q water for 3 × 30 min.

The excessive TiO_2 suspensions were centrifuged. The supernatant clear liquid was decanted and the sludge was blended with Milli-Q water and shaken for washing. After re-sedimentation and decantation, the sludge was dried, pestle, and used for XRD measurements.

3.3. Characterization

For SEM imaging, the samples were sputtered with a 30 nm chromium layer with a Leybold Z400 sputter system (Köln, Germany). Scanning electron microscopy images were taken with a Carl Zeiss Ltd. Ultra 55 SEM (Oberkochen, Germany). X-ray photoelectron spectroscopy spectra were measured at the Kratos Analytical Ltd. Axis Ultra with a monochromatic Al Kα cathode (Manchester, UK). The X-ray source power was 150 W and the pass energy was 40 eV. To gain information about the crystal composition of the TiO_2 nanoparticles XRD measurements were undertaken. It is not possible to directly perform XRD measurements of the TiO_2 layers on the membranes as the signals are superimposed by noise caused by the polymer structure of the membrane. Therefore, the excessive TiO_2 powder in suspension was refined after synthesis and used for XRD. The XRD patterns were measured with a Rigaku Ultima IV X-ray diffraction spectrometer (Tokyo, Japan) with Cu Kα radiation (40 kV, 40 mA, scanning speed: $1° min^{-1}$, step size: $0.02°$). From the peak integrals A, the weight fractions W of the phases were calculated with Equations (1)–(3) using the response factors k ($k_A = 0.886$, $k_R = 1$ and $k_B = 2.721$) [40].

$$W_A = \frac{k_A \cdot A_A}{k_A \cdot A_A + k_R \cdot A_R + k_B \cdot A_B} \tag{1}$$

$$W_R = \frac{k_R \cdot A_R}{k_A \cdot A_A + k_R \cdot A_R + k_B \cdot A_B} \tag{2}$$

$$W_B = \frac{k_B \cdot A_B}{k_A \cdot A_A + k_R \cdot A_R + k_B \cdot A_B} \tag{3}$$

The crystallite sizes of TiO_2 were determined by using Scherrer's equation:

$$d = \frac{0.9\lambda}{(B \cos\theta)} \tag{4}$$

where d, λ, B, and θ are crystallite size, Cu Kα wavelength (0.15418 nm), full width at half–maximum intensity (fwhm) of the reflection (anatase (101), brookite (121), and rutile (110)) in radians, and Bragg's diffraction angle, respectively [64]. For contact angle measurement a piece of modified membrane was glued to an object slide. With a Krüss DSA 30E, a 2 μL water drop was placed on the surface. The process of drop deposition and permeation was tracked by a camera and the contact angle was determined from the video after the drop was completely placed on the membrane. This procedure was repeated on five areas of the membrane. For water permeance measurements membrane circles with a diameter of $d = 2.5$ cm were cut and placed in a Sartorius 16249 pressure filter holder. The time for 100 mL of Milli-Q water passing through the membrane at an applied nitrogen pressure of $p = 1$

bar was measured. For each sample three membrane pieces were tested. From the measured time, the water permeance flux *J* could be calculated using Equation (5):

$$J = \frac{V}{t \times A \times p} \tag{5}$$

where *J* is the permeance flux (mL min^{-1} cm^{-2} bar), *V* is the volume (mL), *t* is time (min), *A* is the surface area of the membrane (cm^2), and *p* is the pressure (bar).

The binding and stability of the TiO$_2$ nanoparticles on the membrane surface was tested by flowing water at high pressure and speed parallel to the membrane surface in a cross-flow mode. A self-build cross-flow setup was used at 100% cross-flow with 30 bar and for 1 h in operation. A possible detachment of TiO$_2$ nanoparticles was analyzed by examining the surface via SEM and XPS before and after the test. Additionally, the passed water was examined to detect possibly leached TiO$_2$ nanoparticles via ICP-OES (SPECTRO Ciros Vision, SPECTRO Analytical Instruments GmbH, Kleve, Germany).

The procedure of the photocatalytic degradation test is described elsewhere [13,14,65]. Briefly, a circle with the diameter d = 2.5 cm was cut from the membrane. An additional hole was cut in the middle of this circle (d = 1 cm) to obtain a ring. Three of these rings were glued into vicinal pits of six-well plates. All six pits were filled with 4 mL of either 13 mg L^{-1} methylene blue or 25 mg L^{-1} carbamazepine solution in water. The zero value of the absorption was measured immediately with a Tecan Infinite M200 multimode microplate reader at a wavelength of 660 nm (methylene blue) or 282 nm (carbamazepine) over a period of 120 min. The samples were shaken on a radial shaker with 200 rpm without irradiation to measure the dark adsorption for 30 min. The absorption of the solution was measured in 10 min intervals. Subsequently, the samples were irradiated with a sunlamp (Heraus Original Hanau Suncare tanning tube 21/25 slim) to perform photocatalysis for 2 h. The radiant flux density of the lamp was 11.3 $\pm$ 1.3 mW cm^{-2}. For the first 40 min, the absorbance was measured every 10 min, afterwards every 20 min. The non-catalytic photolysis was subtracted from the photocatalytic measurement. By plotting log(c/c$_0$) versus the time, observed reaction rate constants *k* could be derived from the slope of the regression line.

4. Conclusions

Highly photocatalytic active TiO$_2$ nanoparticles have been synthesized and were attached to a polymer membrane. The surface was evenly covered with non-agglomerated nanoparticles, which were strongly attached to the membrane.

The crystallinity and photocatalytic activity raises with increasing synthesis temperature. The highest degradation rate (0.11 min^{-1}) was observed at the maximum applied synthesis temperature of 210 °C. The main crystalline phase was anatase with a content between 65% and 85%, while the brookite content varies between 15% and 37%. Rutile only appears at a synthesis temperature of 210 °C with a content of 5%. An even distribution of TiO$_2$ nanoparticles on the surface was achieved by either pre-modifying the membrane with carboxyl groups or ultrasound treatment of TiO$_2$ nanoparticles. The ultrasound treated nanoparticles resulted in the highest photocatalytic activity when degrading carbamazepine. No decrease in photocatalytic activity was observed after nine repetition times. The TiO$_2$ nanoparticles withstand high shear stress due to strong bonding between TiO$_2$ and the PES polymer or the carboxyl group on the membrane, respectively. While the hydrophilicity of the membranes increased (water contact angle below 20°) no significant change of the permeance due to the modification with TiO$_2$ nanoparticles was observed. In conclusion, the TiO$_2$ nanoparticle membrane exhibits excellent stability and performance properties and is therefore suitable to be used for degradation of pollutants in water.

Conflicts of Interest: The authors declare no conflict of interest. The funders had no role in the design of the study; in the collection, analyses, or interpretation of data; in the writing of the manuscript, and in the decision to publish the results.

References

1. Luo, Y.; Guo, W.; Ngo, H.H.; Nghiem, L.D.; Hai, F.I.; Zhang, J.; Liang, S.; Wang, X.C. A review on the occurrence of micropollutants in the aquatic environment and their fate and removal during wastewater treatment. *Sci. Total Environ.* **2014**, *473–474*, 619–641. [CrossRef] [PubMed]

2. Leung, D.Y.C. Outdoor-indoor air pollution in urban environment: Challenges and opportunity. *Front. Environ. Sci.* **2015**, *2*, 69. [CrossRef]

3. Richardson, S.D.; Ternes, T.A. Water analysis: Emerging contaminants and current issues. *Anal. Chem.* **2018**, *90*, 398–428. [CrossRef] [PubMed]

4. Wilkinson, J.; Hooda, P.S.; Barker, J.; Barton, S.; Swinden, J. Occurrence, fate and transformation of emerging contaminants in water: An overarching review of the field. *Environ. Pollut.* **2017**, *231*, 954–970. [CrossRef] [PubMed]

5. Tijani, J.O.; Fatoba, O.O.; Babajide, O.O.; Petrik, L.F. Pharmaceuticals, endocrine disruptors, personal care products, nanomaterials and perfluorinated pollutants: A review. *Environ. Chem. Lett.* **2016**, *14*, 27–49. [CrossRef]

6. Dewil, R.; Mantzavinos, D.; Poulios, I.; Rodrigo, M.A. New perspectives for advanced oxidation processes. *J. Environ. Manag.* **2017**, *195*, 93–99. [CrossRef] [PubMed]

7. Kanakaraju, D.; Glass, B.D.; Oelgemöller, M. Advanced oxidation process-mediated removal of pharmaceuticals from water: A review. *J. Environ. Manag.* **2018**, *219*, 189–207. [CrossRef] [PubMed]

8. Kumar, J.; Bansal, A. Photocatalysis by nanoparticles of titanium dioxide for drinking water purification: A conceptual and state-of-art review. *Mater. Sci. Forum* **2013**, *764*, 130–150. [CrossRef]

9. Molinari, R.; Pirillo, F.; Loddo, V.; Palmisano, L. Heterogeneous photocatalytic degradation of pharmaceuticals in water by using polycrystalline TiO_2 and a nanofiltration membrane reactor. *Catal. Today* **2006**, *118*, 205–213. [CrossRef]

10. Lee, K.M.; Lai, C.W.; Ngai, K.S.; Juan, J.C. Recent developments of zinc oxide based photocatalyst in water treatment technology: A review. *Water Res.* **2016**, *88*, 428–448. [CrossRef] [PubMed]

11. Sarasidis, V.C.; Plakas, K.V.; Patsios, S.I.; Karabelas, A.J. Investigation of diclofenac degradation in a continuous photo-catalytic membrane reactor. Influence of operating parameters. *Chem. Eng. J.* **2014**, *239*, 299–311. [CrossRef]

12. Li, N.; Tian, Y.; Zhang, J.; Sun, Z.; Zhao, J.; Zhang, J.; Zuo, W. Precisely-controlled modification of pvdf membranes with 3d TiO_2/ZnO nanolayer: Enhanced anti-fouling performance by changing hydrophilicity and photocatalysis under visible light irradiation. *J. Membr. Sci.* **2017**, *528*, 359–368. [CrossRef]

13. Fischer, K.; Grimm, M.; Meyers, J.; Dietrich, C.; Gläser, R.; Schulze, A. Photoactive microfiltration membranes via directed synthesis of TiO_2 nanoparticles on the polymer surface for removal of drugs from water. *J. Membr. Sci.* **2015**, *478*, 49–57. [CrossRef]

14. Fischer, K.; Gawel, A.; Rosen, D.; Krause, M.; Abdul Latif, A.; Griebel, J.; Prager, A.; Schulze, A. Low-temperature synthesis of anatase/rutile/brookite TiO_2 nanoparticles on a polymer membrane for photocatalysis. *Catalysts* **2017**, *7*, 209. [CrossRef]

15. Nakata, K.; Fujishima, A. TiO_2 photocatalysis: Design and applications. *J. Photochem. Photobiol. C Photochem. Rev.* **2012**, *13*, 169–189. [CrossRef]

16. Maeda, K. Z-scheme water splitting using two different semiconductor photocatalysts. *ACS Catal.* **2013**, *3*, 1486–1503. [CrossRef]

17. Chen, X.; Li, C.; Gratzel, M.; Kostecki, R.; Mao, S.S. Nanomaterials for renewable energy production and storage. *Chem. Soc. Rev.* **2012**, *41*, 7909–7937. [CrossRef] [PubMed]

18. Pan, X.; Zhao, Y.; Fan, Z. Tio$_2$ nanostructures by electrochemical anodization for dye-sensitized solar cells. *Nanosci. Nanotechnol. Lett.* **2012**, *4*, 463–470. [CrossRef]

19. Zhang, J.; Zhou, P.; Liu, J.; Yu, J. New understanding of the difference of photocatalytic activity among anatase, rutile and brookite TiO$_2$. *Phys. Chem. Chem. Phys.* **2014**, *16*, 20382–20386. [CrossRef] [PubMed]

20. Di Paola, A.; Bellardita, M.; Palmisano, L. Brookite, the least known TiO$_2$ photocatalyst. *Catalysts* **2013**, *3*, 36. [CrossRef]

21. Li, Z.; Cong, S.; Xu, Y. Brookite vs anatase TiO$_2$ in the photocatalytic activity for organic degradation in water. *ACS Catal.* **2014**, *4*, 3273–3280. [CrossRef]

22. Vequizo, J.J.M.; Matsunaga, H.; Ishiku, T.; Kamimura, S.; Ohno, T.; Yamakata, A. Trapping-induced enhancement of photocatalytic activity on brookite TiO$_2$ powders: Comparison with anatase and rutile TiO$_2$ powders. *ACS Catal.* **2017**, *7*, 2644–2651. [CrossRef]

23. Tran, H.T.T.; Kosslick, H.; Ibad, M.F.; Fischer, C.; Bentrup, U.; Vuong, T.H.; Nguyen, L.Q.; Schulz, A. Photocatalytic performance of highly active brookite in the degradation of hazardous organic compounds compared to anatase and rutile. *Appl. Catal. B Environ.* **2017**, *200*, 647–658. [CrossRef]

24. Kandiel, T.A.; Robben, L.; Alkaim, A.; Bahnemann, D. Brookite versus anatase TiO$_2$ photocatalysts: Phase transformations and photocatalytic activities. *Photochem. Photobiol. Sci.* **2013**, *12*, 602–609. [CrossRef] [PubMed]

25. Yu, J.; Wang, B. Effect of calcination temperature on morphology and photoelectrochemical properties of anodized titanium dioxide nanotube arrays. *Appl. Catal. B Environ.* **2010**, *94*, 295–302. [CrossRef]

26. Liao, Y.; Que, W. Preparation and photocatalytic activity of TiO$_2$ nanotube powders derived by a rapid anodization process. *J. Alloys Compd.* **2010**, *505*, 243–248. [CrossRef]

27. Kim, S.-J.; Lee, E.G.; Park, S.D.; Jeon, C.J.; Cho, Y.H.; Rhee, C.K.; Kim, W.W. Photocatalytic effects of rutile phase TiO$_2$ ultrafine powder with high specific surface area obtained by a homogeneous precipitation process at low temperatures. *J. Sol-Gel Sci. Technol.* **2001**, *22*, 63–74. [CrossRef]

28. Cao, Y.; Li, X.; Bian, Z.; Fuhr, A.; Zhang, D.; Zhu, J. Highly photocatalytic activity of brookite/rutile TiO$_2$ nanocrystals with semi-embedded structure. *Appl. Catal. B Environ.* **2016**, *180*, 551–558. [CrossRef]

29. Ozawa, T.; Iwasaki, M.; Tada, H.; Akita, T.; Tanaka, K.; Ito, S. Low-temperature synthesis of anatase–brookite composite nanocrystals: The junction effect on photocatalytic activity. *J. Colloid Interface Sci.* **2005**, *281*, 510–513. [CrossRef] [PubMed]

30. Allen, N.S.; Mahdjoub, N.; Vishnyakov, V.; Kelly, P.J.; Kriek, R.J. The effect of crystalline phase (anatase, brookite and rutile) and size on the photocatalytic activity of calcined polymorphic titanium dioxide (TiO$_2$). *Polym. Degrad. Stab.* **2018**, *150*, 31–36. [CrossRef]

31. Gao, Y.; Wang, H.; Wu, J.; Zhao, R.; Lu, Y.; Xin, B. Controlled facile synthesis and photocatalytic activity of ultrafine high crystallinity TiO$_2$ nanocrystals with tunable anatase/rutile ratios. *Appl. Surf. Sci.* **2014**, *294*, 36–41. [CrossRef]

32. Cano-Casanova, L.; Amorós-Pérez, A.; Ouzzine, M.; Lillo-Ródenas, M.A.; Román-Martínez, M.C. One step hydrothermal synthesis of TiO$_2$ with variable hcl concentration: Detailed characterization and photocatalytic activity in propene oxidation. *Appl. Catal. B Environ.* **2018**, *220*, 645–653. [CrossRef]

33. Štengl, V.; Králová, D. Photoactivity of brookite–rutile TiO$_2$ nanocrystalline mixtures obtained by heat treatment of hydrothermally prepared brookite. *Mater. Chem. Phys.* **2011**, *129*, 794–801. [CrossRef]

34. Bai, H.; Zan, X.; Zhang, L.; Sun, D.D. Multi-functional CNT/ZnO/TiO$_2$ nanocomposite membrane for concurrent filtration and photocatalytic degradation. *Sep. Purif. Technol.* **2015**, *156*, 922–930. [CrossRef]

35. Madaeni, S.S.; Zinadini, S.; Vatanpour, V. A new approach to improve antifouling property of pvdf membrane using in situ polymerization of paa functionalized TiO$_2$ nanoparticles. *J. Membr. Sci.* **2011**, *380*, 155–162. [CrossRef]

36. Wu, M.; Lin, G.; Chen, D.; Wang, G.; He, D.; Feng, S.; Xu, R. Sol-hydrothermal synthesis and hydrothermally structural evolution of nanocrystal titanium dioxide. *Chem. Mater.* **2002**, *14*, 1974–1980. [CrossRef]

37. Cheng, H.; Ma, J.; Zhao, Z.; Qi, L. Hydrothermal preparation of uniform nanosize rutile and anatase particles. *Chem. Mater.* **1995**, *7*, 663–671. [CrossRef]

38. Hegazy, A.; Kinadjian, N.; Sadeghimakki, B.; Sivoththaman, S.; Allam, N.K.; Prouzet, E. Tio$_2$ nanoparticles optimized for photoanodes tested in large area dye-sensitized solar cells (dssc). *Sol. Energy Mater. Sol. Cells* **2016**, *153*, 108–116. [CrossRef]

39. Yanagisawa, K.; Ovenstone, J. Crystallization of anatase from amorphous titania using the hydrothermal technique: Effects of starting material and temperature. *J. Phys. Chem. B* **1999**, *103*, 7781–7787. [CrossRef]

40. Liu, C.; Yu, T.; Tan, X. Characterization and photocatalytic activity of mixed nanocrystalline TiO_2 powders prepared by xerogel-hydrothermal method in different acid solutions. *Trans. Tianjin Univ.* **2016**, *22*, 473–479. [CrossRef]

41. Yin, S.; Hasegawa, H.; Maeda, D.; Ishitsuka, M.; Sato, T. Synthesis of visible-light-active nanosize rutile titania photocatalyst by low temperature dissolution–reprecipitation process. *J. Photochem. Photobiol. A Chem.* **2004**, *163*, 1–8. [CrossRef]

42. Yin, H.; Wada, Y.; Kitamura, T.; Kambe, S.; Murasawa, S.; Mori, H.; Sakata, T.; Yanagida, S. Hydrothermal synthesis of nanosized anatase and rutile TiO_2 using amorphous phase TiO_2. *J. Mater. Chem.* **2001**, *11*, 1694–1703. [CrossRef]

43. Li, Y.; Fan, Y.; Chen, Y. A novel method for preparation of nanocrystalline rutile TiO_2 powders by liquid hydrolysis of ticl4. *J. Mater. Chem.* **2002**, *12*, 1387–1390. [CrossRef]

44. Bignold, G.J.; Brewer, A.D.; Hearn, B. Specific conductivity and ionic product of water between 50 and 271 °C. *Trans. Faraday Soc.* **1971**, *67*, 2419–2430. [CrossRef]

45. Neppolian, B.; Wang, Q.; Jung, H.; Choi, H. Ultrasonic-assisted sol-gel method of preparation of TiO_2 nano-particles: Characterization, properties and 4-chlorophenol removal application. *Ultrason. Sonochem.* **2008**, *15*, 649–658. [CrossRef] [PubMed]

46. Schulze, A.; Maitz, M.F.; Zimmermann, R.; Marquardt, B.; Fischer, M.; Werner, C.; Went, M.; Thomas, I. Permanent surface modification by electron-beam-induced grafting of hydrophilic polymers to pvdf membranes. *RSC Adv.* **2013**, *3*, 22518–22526. [CrossRef]

47. Luo, M.-L.; Zhao, J.-Q.; Tang, W.; Pu, C.-S. Hydrophilic modification of poly(ether sulfone) ultrafiltration membrane surface by self-assembly of TiO_2 nanoparticles. *Appl. Surf. Sci.* **2005**, *249*, 76–84. [CrossRef]

48. Qian, Y.; Chi, L.; Zhou, W.; Yu, Z.; Zhang, Z.; Zhang, Z.; Jiang, Z. Fabrication of TiO_2-modified polytetrafluoroethylene ultrafiltration membranes via plasma-enhanced surface graft pretreatment. *Appl. Surf. Sci.* **2015**, *360*, 749–757. [CrossRef]

49. Khulbe, K.C.; Feng, C.; Matsuura, T. The art of surface modification of synthetic polymeric membranes. *J. Appl. Polym. Sci.* **2010**, *115*, 855–895. [CrossRef]

50. Breite, D.; Went, M.; Prager, A.; Schulze, A. Tailoring membrane surface charges: A novel study on electrostatic interactions during membrane fouling. *Polymers* **2015**, *7*, 1497. [CrossRef]

51. Wavhal, D.S.; Fisher, E.R. Hydrophilic modification of polyethersulfone membranes by low temperature plasma-induced graft polymerization. *J. Membr. Sci.* **2002**, *209*, 255–269. [CrossRef]

52. Ibrahim, H.M.M. Photocatalytic degradation of methylene blue and inactivation of pathogenic bacteria using silver nanoparticles modified titanium dioxide thin films. *World J. Microbiol. Biotechnol.* **2015**, *31*, 1049–1060. [CrossRef] [PubMed]

53. Thongrom, B.; Amornpitoksuk, P.; Suwanboon, S.; Baltrusaitis, J. Photocatalytic degradation of dye by Ag/ZnO prepared by reduction of tollen's reagent and the ecotoxicity of degraded products. *Korean J. Chem. Eng.* **2014**, *31*, 587–592. [CrossRef]

54. Chakraborty, S.; Loutatidou, S.; Palmisano, G.; Kujawa, J.; Mavukkandy, M.O.; Al-Gharabli, S.; Curcio, E.; Arafat, H.A. Photocatalytic hollow fiber membranes for the degradation of pharmaceutical compounds in wastewater. *J. Environ. Chem. Eng.* **2017**, *5*, 5014–5024. [CrossRef]

55. Wang, J.; Zhao, H.; Liu, X.; Li, X.; Xu, P.; Han, X. Formation of ag nanoparticles on water-soluble anatase TiO_2 clusters and the activation of photocatalysis. *Catal. Commun.* **2009**, *10*, 1052–1056. [CrossRef]

56. Chen, F.; Li, S.; Chen, Q.; Zheng, X.; Liu, P.; Fang, S. 3D graphene aerogels-supported ag and ag@ag3po4 heterostructure for the efficient adsorption-photocatalysis capture of different dye pollutants in water. *Mater. Res. Bull.* **2018**, *105*, 334–341. [CrossRef]

57. Suttiponparnit, K.; Jiang, J.; Sahu, M.; Suvachittanont, S.; Charinpanitkul, T.; Biswas, P. Role of surface area, primary particle size, and crystal phase on titanium dioxide nanoparticle dispersion properties. *Nanoscale Res. Lett.* **2010**, *6*, 27. [CrossRef] [PubMed]

58. Zhang, Y.; Geißen, S.-U.; Gal, C. Carbamazepine and diclofenac: Removal in wastewater treatment plants and occurrence in water bodies. *Chemosphere* **2008**, *73*, 1151–1161. [CrossRef] [PubMed]

59. McEneff, G.; Barron, L.; Kelleher, B.; Paull, B.; Quinn, B. A year-long study of the spatial occurrence and relative distribution of pharmaceutical residues in sewage effluent, receiving marine waters and marine bivalves. *Sci. Total Environ.* **2014**, *476–477*, 317–326. [CrossRef] [PubMed]

60. Ramasundaram, S.; Seid, M.G.; Kim, H.-E.; Son, A.; Lee, C.; Kim, E.-J.; Hong, S.W. Binder-free immobilization of TiO_2 photocatalyst on steel mesh via electrospraying and hot-pressing and its application for organic micropollutant removal and disinfection. *J. Hazard. Mater.* **2018**, *360*, 62–70. [CrossRef] [PubMed]

61. Gaya, U.I.; Abdullah, A.H. Heterogeneous photocatalytic degradation of organic contaminants over titanium dioxide: A review of fundamentals, progress and problems. *J. Photochem. Photobiol. C Photochem. Rev.* **2008**, *9*, 1–12. [CrossRef]

62. Jelic, A.; Michael, I.; Achilleos, A.; Hapeshi, E.; Lambropoulou, D.; Perez, S.; Petrovic, M.; Fatta-Kassinos, D.; Barcelo, D. Transformation products and reaction pathways of carbamazepine during photocatalytic and sonophotocatalytic treatment. *J. Hazard. Mater.* **2013**, *263*, 177–186. [CrossRef] [PubMed]

63. Petrochenko, P.; Scarel, G.; Hyde, G.K.; Parsons, G.; Skoog, S.; Zhang, Q.; Goering, P.; Narayan, R. Prevention of ultraviolet (uv)-induced surface damage and cytotoxicity of polyethersulfone using atomic layer deposition (ald) titanium dioxide. *JOM* **2013**, *65*, 550–556. [CrossRef]

64. Yuwono, A.H.; Sofyan, N.; Kartini, I.; Ferdiansyah, A.; Pujianto, T.H. Nanocrystallinity enhancement of TiO_2 nanotubes by post-hydrothermal treatment. *Adv. Mater. Res.* **2011**, *277*, 90–99. [CrossRef]

65. Fischer, K.; Gläser, R.; Schulze, A. Nanoneedle and nanotubular titanium dioxide—Pes mixed matrix membrane for photocatalysis. *Appl. Catal. B Environ.* **2014**, *160–161*, 456–464. [CrossRef]